This is the preprint version of the article:
S. R. Nekoo, A. Suarez, J. Á. Acosta, G. Heredia and A. Ollero, "Constrained Design Optimization of a Long-Reach Dual-Arm Aerial Manipulator for Maintenance Tasks," 2023 International Conference on Unmanned Aircraft Systems (ICUAS), Warsaw, Poland, 2023, pp. 281-288, doi: 10.1109/ICUAS57906.2023.10156252.

Constrained Design Optimization of a Long-Reach Dual-Arm Aerial Manipulator for Maintenance Tasks

Saeed Rafee Nekoo, Alejandro Suarez, José Ángel Acosta, Guillermo Heredia and Anibal Ollero
GRVC Robotics Lab., Departamento de Ingeniería de Sistemas y Automática
Escuela Técnica Superior de Ingeniería, Universidad de Sevilla, Seville, Spain
Emails: saerafee@yahoo.com, (asuarezfm, jaar, guiller, aollero)@us.es

***Abstract*—Motivated by the convenience of improving the performance of long-reach aerial manipulators in the realization of maintenance tasks on high-voltage power lines, this paper proposes a constrained design optimization method for dual-arm aerial manipulators intended to reduce the weight while increasing the workspace of the robot. This configuration, in which the arms are separated from the aerial platform through a long reach link similar to a pendulum, improves safety in the interaction with human workers, reduces the electromagnetic interference of high voltage power lines on the electronics, as well as the aerodynamic downwash effect due to the propellers. However, the long-reach link introduces undesired vibrations on the manipulator due to its flexibility, so its length imposes a trade-off between the safety of operation as a positive side-effect and vibration as a negative one. Therefore, the cost function in the optimization problem also accounts for this factor, limiting the vibration to a fixed predefined value. A recent optimization approach is used here to minimize the cost function and solve the problem, verified by particle swarm optimization as a basis to confirm the correctness of the obtained data.**

Keywords— Long-reach aerial manipulator; Constrained optimization; Search algorithm; Particle swarm optimization.

I. INTRODUCTION

The inspection and maintenance (I&M) of power lines is an illustrative application example where the use of aerial manipulation robots – drones equipped with robotic arms – may contribute to reducing significantly the time, cost, and risk in the realization of these operations concerning current solutions carried out by human operators working in high-risk conditions. The installation of bird-flight diverters and other devices like spacers or anti-vibrators (depicted in Fig. 1), the insulation of the cables of the power lines, or the replacement of damaged devices are some typical tasks that require the deployment of the operators in these high altitude workspaces, using heavy vehicles like manned helicopters, cranes or elevated work platforms to reach and operate on the power lines. Given the vast extension of this infrastructure (a single country counts hundreds of thousands of kilometers of power lines), and the need to conduct periodic I&M campaigns to evaluate the state of the different elements, it is highly desirable to explore the use of alternative technological solutions that may obtain a significant benefit for the companies in charge of their management. In this sense, the aerial manipulation field has demonstrated the possibility to conduct many operations and tasks on the flight, integrating robotic manipulators in vertical take-off and landing UAVs (unmanned aerial vehicles) like multirotor and autonomous helicopters to facilitate access to remote or high-altitude workspace [1-3]. The inspection by contact of pipes, tanks, and other surfaces [4-6], the installation and retrieval of sensor devices [7], the valve turning [8], and other torsional operations [9], the inspection of bridges [10], or the grasping [11-13], are some examples of capabilities and functionalities of this kind of robots.

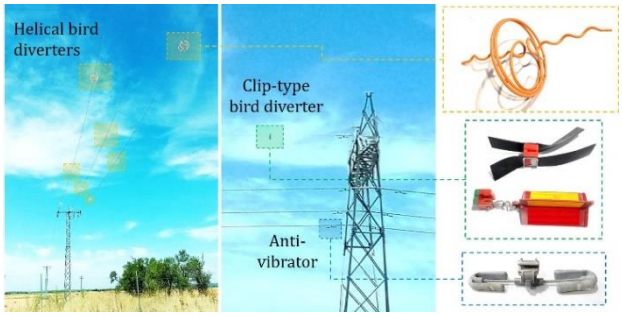

Fig. 1. Different devices typically installed on high-voltage power lines require periodic maintenance.

Since aerial robotic manipulators are intended to interact physically with the environment, the risk of collision of the propellers with the surrounding obstacles is considerable taking into account that the manipulator is usually placed as close as possible to the multirotor base to reduce the effect of the interaction wrenches. Note that the reach of the end-effector is typically within the perimeter of the propellers [14]; also the effective workspace of the system is constrained by the landing gear [15-17]. The risk of collision is even higher in outdoor scenarios due to the low accuracy of the positioning systems compared to Vicon or Opti Track systems employed in indoor testbeds; other undesirable effects are wind gusts or unexpected contact forces. This motivated the introduction of aerial manipulators in long-reach (also known as a passive pendulum or swing) configurations [7] to improve safety during the interactions on a flight in three ways: 1) by increasing the separation distance between the propellers and the obstacles close to the workspace, and with it, the reaction time, 2) by preventing from transmission of contact force to the multirotor base as a moment, but as a force, through the passive joint at the base, and 3) by extending the effective workspace of the arms, removing the motion constraints associated to the multirotor frame [14].

This is the preprint version of the article:
S. R. Nekoo, A. Suarez, J. Á. Acosta, G. Heredia and A. Ollero, "Constrained Design Optimization of a Long-Reach Dual-Arm Aerial Manipulator for Maintenance Tasks," 2023 International Conference on Unmanned Aircraft Systems (ICUAS), Warsaw, Poland, 2023, pp. 281-288, doi: 10.1109/ICUAS57906.2023.10156252.

The design of a dual-arm aerial manipulator requires the definition of several geometric parameters. The increase in the workspace of the arms by increasing the length of the link is desirable, though it leads to extra weight for the multi-rotor and more significant vibrations. This arise the formulation of an optimization problem for the design of the proposed system. The definition of the cost function for optimization of the aerial robot with mentioned capabilities presents a very complex objective function, not necessarily convex, with many constraints. Solving such optimization problems is not easy through mathematical optimization tools such as the gradient descent method [18], convex programming [19], linear programming [20], and social group optimization [21], etc. have been investigated. The heuristic-metaheuristic search methods are powerful approaches to optimizing complex cost functions, unlike mathematically based methods, they do not guarantee convergence [22]. The application of metaheuristic search is quite vast in different disciplines. Ghosh et al. [23] used a recursive memetic algorithm for medical purposes, searching for gene selection in microarray data. Application of metaheuristics in engineering was also extensive though the focus is on aerial robotics. Alfeo et al. used metaheuristics for enhancing biologically inspired swarm behavior for many small UAVs in a search mission in an unknown environment [24]. Mahanta et al. employed particle swarm optimization and an artificial bee colony to perform design optimization for the gripper of the manipulator [25]. The cost function of the problem was complex, acting as a multi-objective constraint optimization problem with seven decision variables. A two-layer metaheuristics optimization was presented for multi-robot aerial systems [26].

The main contribution of this work is the definition of a systematic way for designing the cost function of a dual-arm long-reach aerial manipulator, employing a search algorithm for design optimization [27]. The objective function of the optimization includes static characteristics such as the weight, geometry, and workspace of the robot, as well as dynamic characteristics like vibration control. The search algorithm proposed in [27] works by introducing random solutions in the workspace and systematically reducing the search domain to reach the best answer. The proposed method can be extended to incorporate other optimization criteria, such as the payload capacity of the arms.

Section II motivates the adoption of long-reach aerial manipulators and describes the considered system. Section III states the cost function and constraints. Section IV presents the inspiration and pseudocode of the search algorithm, whereas Section V is focused on particle swarm optimization. Simulation results are reported in Section VI, and the conclusions are in Section VII.

II. Description of the Long-Reach Aerial Manipulator

A. Motivation

As stated before, long-reach aerial manipulators (LRAM) in passive pendulum (or swing) configuration aim to improve safety in the realization of manipulation tasks on a flight by increasing the separation distance between the aerial platform and the environmental obstacles close to the end-effectors. Fig. 2 illustrates its application in the installation of a helical bird flight diverter on a power line with a dual-arm aerial manipulator, comparing both the standard and long-reach configurations [7]. The LRAM consists of three main parts: the aerial platform, the robotic manipulator, and the long-reach link that connects both parts, which is supported by a passive joint attached to the multirotor base. The passive joint avoids the transmission of torques from the manipulator to the aerial platform at a pitch angle, benefitting the attitude controller, whereas the lateral deflection of the long reach link, built with a simple aluminum profile [28], provides a certain level of accommodation to the lateral contact forces that may induce a torque in the roll angle, as illustrated in Fig. 2. Note that, unlike the cable-suspended aerial manipulators [29, 30], the passive joint constrains the free motion of the manipulator to a single axis rotation, which is convenient in terms of controllability. Experimental results revealed that the oscillations of the long reach link (caused by the acceleration of the pendulum or other maneuvers like the take-off) were attenuated faster when the aerial robot was flying in the fixed base, as the floating platform tended to dissipate the potential energy stored in the pendulum as kinetic energy [28].

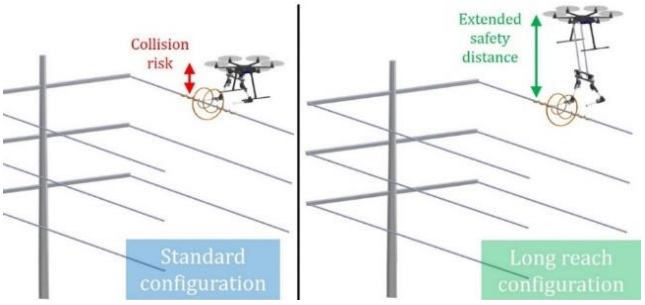

Fig. 2. Comparison of aerial manipulation robot manipulating a helical bird flight diverter on a power line, considering the standard (left) and long reach (right) configurations.

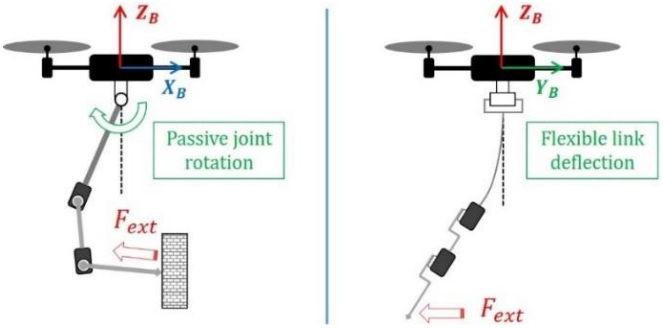

Fig. 3. Passive joint rotation and flexible link deflection are caused by an external force applied at the end-effector of the manipulator.

B. System Description

The manipulator considered in this work is a lightweight and compliant dual-arm system, shown in Fig. 4, whose main features are indicated in Table 1. The arms, specifically designed for their integration in medium-scale multi-rotors,

This is the preprint version of the article:
S. R. Nekoo, A. Suarez, J. Á. Acosta, G. Heredia and A. Ollero, "Constrained Design Optimization of a Long-Reach Dual-Arm Aerial Manipulator for Maintenance Tasks," 2023 International Conference on Unmanned Aircraft Systems (ICUAS), Warsaw, Poland, 2023, pp. 281-288, doi: 10.1109/ICUAS57906.2023.10156252.

are built with the Herkulex DRS-0201 smart servo actuators and a customized frame structure manufactured in aluminum and carbon fiber. The long-reach link consists of a pair of $15 \times 2 \times 450$ mm anodized aluminum profiles separated by a distance of 140 mm. The tip of these two profiles is supported by a passive joint at the base of the multi-rotor, facilitating in this way the take-off and landing, as depicted in Fig. 5. The Denavit-Hartenberg parameters of the arms and the reference frames are represented in Fig. 6 and Table 2, respectively.

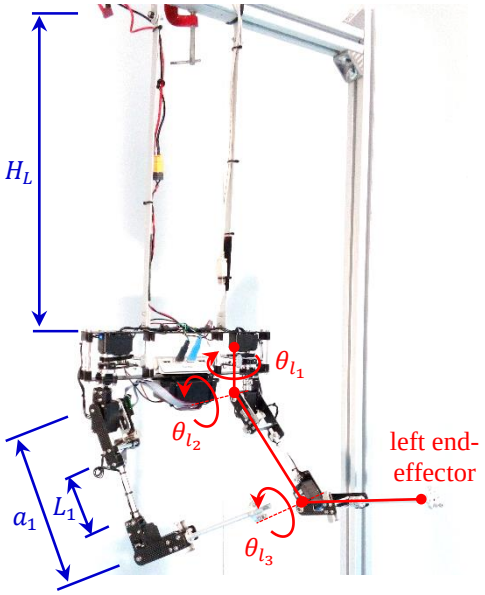

Fig. 4. Parameters definition of the prototype.

Table 1. Main features of the dual-arm system.

Weight	Total	1.0	kg
Lift load capacity	At elbow joint	0.4	kg
	At shoulder joint	0.15	kg
Dimensions	Long reach link	450	mm
	Forearm link	200	mm
	Upper arm link	200	mm
	Arms separation	250	mm
Joint stall torque	In all joints	2.4	Nm
Joint stiffness	In all joints	4.2	Nm/rad
Max. joint speed	In all joints	300	degree/s
Joint deflection	In all joints	≤15	degree
Power supply	Dual-arm	7.4 – 9	V

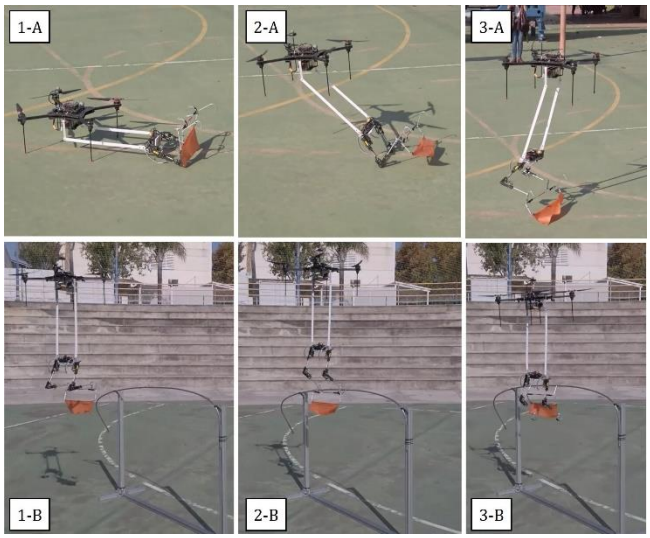

Fig. 5. Dual-arm aerial manipulator in long reach configuration: take-off sequence (up), and installation of bird diverter on the power line (down).

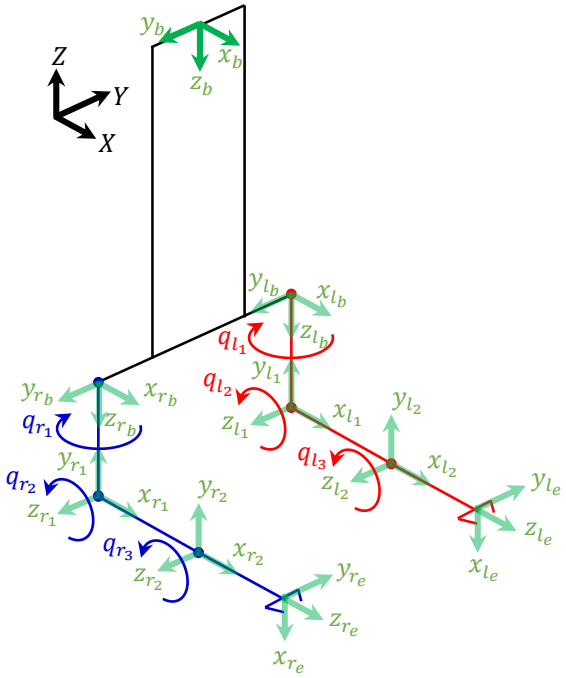

Fig. 6. The Denavit-Hartenberg parameters of the system.

Table 2. The Denavit-Hartenberg parameters of the dual-arm system.

Joint	d (m)	a (m)	θ (rad)	α (rad)
1	0.11	0	q_1	$-\pi/2$
2	0	0.2	q_2	0
3	0	0.2	q_3	0

The arms implement the classical kinematic configuration with three joints for end-effector positioning: shoulder yaw (base), shoulder pitch, and elbow pitch. It should be noted that $a_i(\mathrm{m})$ represents the distance between two joints while $L_i(\mathrm{m})$ denotes the aluminum part of the link (variable part in the

This is the preprint version of the article:
S. R. Nekoo, A. Suarez, J. Á. Acosta, G. Heredia and A. Ollero, "Constrained Design Optimization of a Long-Reach Dual-Arm Aerial Manipulator for Maintenance Tasks," 2023 International Conference on Unmanned Aircraft Systems (ICUAS), Warsaw, Poland, 2023, pp. 281-288, doi: 10.1109/ICUAS57906.2023.10156252.

optimization process). In order to increase the workspace, the accessibility of end-effector positions must be expanded. The forward kinematics is used to find the end-effector position in the Cartesian coordinate:

$$x_{\mathrm{e},i} = \cos q_{1,i}\left(a_3\cos(q_{2,i}+q_{3,i}) + a_2\cos q_{2,i}\right),$$
$$y_{\mathrm{e},i} = \pm d/2 + \sin q_{1,i}\left(a_3\cos(q_{2,i}+q_{3,i}) + a_2\cos q_{2,i}\right),$$
$$z_{\mathrm{e},i} = -d_1 - H_L + a_3\sin(q_{2,i}+q_{3,i}) + a_2\sin q_{2,i},$$

where $i=\{l,r\}$ is the left/right arm index, $\{q_{1,i}, q_{2,i}, q_{3,i}\}$ are the generalized coordinates, d_1, a_2, a_3 (m) are the length of the links with respect, d (m) is the distance between the arms and H_L (m) is the length of the aluminum frame.

III. Cost Function and Constraints

The objective of the optimization problem addressed here is to determine the lengths of the links for the dual-arm with the maximum possible workspace, taking into account the trade-off between workspace, weight, and also the vibration caused by the flexibility of the long reach link that connects the arms with the multi-rotor. Formulating a good objective function for optimization guides the design to the best solution. The overall cost function must include minimization of the total mass, maximization of the arms workspace, and keeping the vibration within the allowable bound:

$$\text{minimize: } F(\mathbf{x}) = M(\mathbf{x}) + \frac{Q}{W(\mathbf{x})} + \frac{1}{V(\mathbf{x})}, \tag{1}$$

where $\mathbf{x}=[x_1, x_2, \dots, x_n]^T$ collects n variables of the optimization related to geometry, $M(\mathbf{x})$ is the total mass objective function, $W(\mathbf{x})$ is the workspace function, and $V(\mathbf{x})$ is the vibration control cost function. The mass $M(\mathbf{x})$ should be minimized and workspace $W(\mathbf{x})$ should be maximized. The trade-off between workspace, mass, and vibration, in Eq. (1), is done by scaling factor Q.

The first part of the cost function is the total mass of the system, which comprises on the one hand the fixed-weight components such as the servomotors, carbon fiber frame parts, screws, and nuts, and on the other hand, those elements with variable length/weight, which are aluminum tubes of links and the flexible long reach link of the dual-arm system:

$$M(\mathbf{x}) = M_{\mathrm{f}}(\mathbf{x}) + M_{\mathrm{t}}(\mathbf{x}) + M_{\mathrm{e}}, \tag{2}$$

where $M_{\mathrm{f}}(\mathbf{x})$ is the mass of the aluminum frame, $M_{\mathrm{t}}(\mathbf{x})$ is the mass of aluminum tubes (links), and M_{e} is the mass of the rest of the elements. The nominal value of the current design sums up the total mass $M_{\mathrm{nom}} = 1$ (kg).

The cross-sectional area of the connecting aluminum frame is a rectangle of height b (m) and thickness t (m). The total length of the connecting frame is $L_{\mathrm{f}} = 2L_3$ (m) in which L_3 is the height of the frame. The total mass of the frame is $M_{\mathrm{f}}(\mathbf{x}) = \rho b t L_{\mathrm{f}}$ where $\rho = 2720\ (kg/m^3)$ is the density of aluminum alloy 6061. The mass of aluminum tubes of the dual arm is $M_{\mathrm{t}}(\mathbf{x}) = \rho\frac{\pi}{4}(D^2-d^2)\times 2(L_1+L_2)$ where D (m) is the outer diameter of the tube, d (m) is the inner diameter, L_1 (m) is the length of the first tube and L_2 (m) is for the second link.

It should be noted that the total length of the links is the summation of the length of the motor installation L_{m_i} (m) and aluminum tube L_i which introduces $a_i = L_{m_i} + L_i$ for $i=\{1,2\}$ (see Fig. 4 and 6). The rest of the equipment such as motors and encoders, etc. is introduced by $M_{\mathrm{e}} = 0.895$ (kg).

The workspace is the second item in the overall objective function. Workspace analysis is a complex subject with joint limitations. The long-reach manipulator is in the category of the spherical robot with articulated joints. The maximum bound of the workspace of the such arm is a sphere, provided that joint limitation is ignored. The radius of the sphere is $R = a_2 + a_3$. The system is a dual-arm manipulator hence the workspace to be maximized is:

$$W(\mathbf{x}) = 2\frac{4}{3}\pi R^3\ (\mathrm{m}^3). \tag{3}$$

One mode of design of the long-reach manipulator is like a pendulum to avoid transmission of the UAV's unsteady motions to the operating dual-arm manipulator. In pendulum mode, low-amplitude force interaction with the environment and the power line is intended. The second mode is working with high-amplitude force, clamped-free mode, where a locker limits the rotary motion of the connecting framework. These operation modes are compared in Fig. 7.

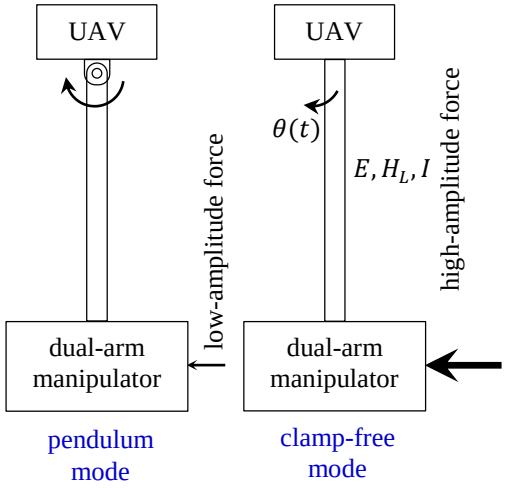

Fig. 7. Illustration of pendulum and clamp-free mode.

The vibration optimization design is based on the clamped-free mode, interacting with the environment with a high-amplitude force. There is a working condition for the dual-arm system; it should interact with an environment that imposes a high-amplitude alternating load. The simplified model of the dynamic load is considered as $F_{\mathrm{e}}(t) = F_0\sin\omega t$ (N) where ω (rad/s) is the frequency of the load and F_0 is the amplitude. The presented clamp-free system in Fig. 7 could be modeled by an equivalent mass-spring-damper system, possessing one degree of freedom in which $K_{\mathrm{eq}}(\mathbf{x}) = 2\frac{3EI(\mathbf{x})}{H_L^3}\left(\frac{\mathrm{N}}{\mathrm{m}}\right)$ is the spring constant of the system; there are 2 aluminum

This is the preprint version of the article:
S. R. Nekoo, A. Suarez, J. Á. Acosta, G. Heredia and A. Ollero, "Constrained Design Optimization of a Long-Reach Dual-Arm Aerial Manipulator for Maintenance Tasks," 2023 International Conference on Unmanned Aircraft Systems (ICUAS), Warsaw, Poland, 2023, pp. 281-288, doi: 10.1109/ICUAS57906.2023.10156252.

connecting links so $\frac{3EI(\mathbf{x})}{H_L^3}$ is doubled, $E = 68.9 \times 10^9$ (Pa) is elasticity modulus, and $I(\mathbf{x}) = \frac{tb^3}{12}$ (m^4) is the second moment of the cross-sectional area of the connecting link. The limiting locker of the long-reach manipulator imposes an estimated constant $C_{\mathrm{eq}} = 200\ \left(\frac{\mathrm{Nms}}{\mathrm{rad}}\right)$ damping characteristics to the equation and equivalent inertia is $I_{\mathrm{eq}}(\mathbf{x}) = \frac{M_{\mathrm{f}}(\mathbf{x})L_{\mathrm{f}}^2(\mathbf{x})}{3} + (M_{\mathrm{t}}(\mathbf{x}) + M_{\mathrm{e}})L_{\mathrm{f}}^2(\mathbf{x})$ (kgm^2). The equation of motion of the equivalent system is:

$$I_{\mathrm{eq}}(\mathbf{x})\ddot{\theta}(t) + C_{\mathrm{eq}}\dot{\theta}(t) + K_{\mathrm{eq}}(\mathbf{x})\theta(t) = F_{\mathrm{e}}(t), \tag{4}$$

where $\theta(t)$ (rad) is the deflection angle of the loaded beam in Fig. 7. The vibration control design is to keep the deflection angle $\theta(t) < \theta_{\max}$. The dynamic load factor is used to impose this condition. The definition of the factor is $R_{\mathrm{d}}(\mathbf{x}) = \frac{1}{\sqrt{(1-r^2(\mathbf{x}))^2+(2\zeta(\mathbf{x})r(\mathbf{x}))^2}}$ where $r(\mathbf{x}) = \frac{\omega}{\omega_{\mathrm{n}}}$ is frequency ratio, $\omega\ \left(\frac{\mathrm{rad}}{\mathrm{s}}\right)$ is load frequency, $\omega_{\mathrm{n}} = \sqrt{\frac{K_{\mathrm{eq}}(\mathbf{x})}{I_{\mathrm{eq}}(\mathbf{x})}}\ \left(\frac{\mathrm{rad}}{\mathrm{s}}\right)$ is natural frequency of the system (4), and $\zeta(\mathbf{x}) = \frac{C_{\mathrm{eq}}}{2\sqrt{K_{\mathrm{eq}}(\mathbf{x})I_{\mathrm{eq}}(\mathbf{x})}}$ is damping ratio. The definition of dynamic load factor is:

$$R_{\mathrm{d}}(\mathbf{x}) = \frac{[\theta_{\max}]_{\mathrm{dynamic}}}{[\theta_{\max}]_{\mathrm{static}}} = \frac{1}{\sqrt{(1-r^2(\mathbf{x}))^2 + (2\zeta(\mathbf{x})r(\mathbf{x}))^2}}.$$

The maximum static deflection angle is $[\theta_{\max}]_{\mathrm{static}} = \frac{F_0}{K_{\mathrm{eq}}(\mathbf{x})}$ and the maximum allowable dynamic deflection angle is $[\theta_{\max}]_{\mathrm{dynamic}} = \theta_{\max}$, hence $\theta_{\max} = R_{\mathrm{d}}(\mathbf{x})F_0/K_{\mathrm{eq}}(\mathbf{x})$, which defines the vibration cost function in Eq. (1) as:

$$\begin{aligned} V(\mathbf{x}) &= \frac{R_{\mathrm{d}}(\mathbf{x})F_0}{K_{\mathrm{eq}}(\mathbf{x})} + H_L^2 \\ &= \frac{F_0}{K_{\mathrm{eq}}(\mathbf{x})\sqrt{(1-r^2(\mathbf{x}))^2 + (2\zeta(\mathbf{x})r(\mathbf{x}))^2}} + H_L^2, \end{aligned} \tag{5}$$

where H_L^2 is added to maximize the distance between the dual arm and the drone as well. The constraints are rooted in vibration limits and geometry. The first one is the maximum allowable dynamic deflection of the aluminum frame which leads to:

$$g_1(\mathbf{x}) = \frac{R_{\mathrm{d}}(\mathbf{x})F_0}{K_{\mathrm{eq}}(\mathbf{x})\theta_{\max}} - 1 \le 0.$$

The geometric constraint also implies that $t < b$, $d < D$, $L_2 < L_1$, and the difference between the inner and outer diameters of the aluminum tubes is 2 mm. These limitations result in:

$$g_2(\mathbf{x}) = \frac{t}{b} - 1 \le 0, g_3(\mathbf{x}) = \frac{d}{D} - 1 \le 0,$$
$$g_4(\mathbf{x}) = (D-d) - 0.002 = 0, g_5(\mathbf{x}) = \frac{L_2}{L_1} - 1 \le 0.$$

The variables of the optimization problem are set as $\mathbf{x} = [x_1, x_2, \dots, x_7]^T = [L_3, b, t, L_1, L_2, D, d]^T$ and the limits of them are $\mathbf{x}_{\min} = [0.4, 0.01, 0.002, 0.1, 0.1, 0.004, 0.002]^T$ and $\mathbf{x}_{\max} = [0.6, 0.02, 0.006, 0.18, 0.18, 0.012, 0.008]^T$. The parameters of the optimization are defined: the amplitude of the load as $F_0 = 25$ (N), load frequency $\omega = 25\ \left(\frac{\mathrm{rad}}{\mathrm{s}}\right)$, fixed length of the first link $d_1 = 0.11$ (m), length of motor installation $L_{m_1} = 0.09$ (m) and $L_{m_2} = 0.06$ (m), the maximum allowable deflection angle $\theta_{\max} = 0.25^{\circ}$ and scale factor as $Q = 0.25$. Substituting all the parameters and the functions of the optimization problem in Eqs. (2), (3), and (5), the total cost function (1) is rewritten as

$$\text{minimize: } F(\mathbf{x}) = F_1(\mathbf{x}) + F_2(\mathbf{x}) + F_3(\mathbf{x}), \tag{6}$$

where

$$F_1(\mathbf{x}) = 1360\pi(x_4 + x_5)(x_6^2 - x_7^2) + 5440x_1x_2x_3 + 0.895,$$
$$F_2(\mathbf{x}) = \frac{3 \times Q}{8\pi(x_4 + x_5 + 0.26)^3},$$
$$\begin{aligned} F_3(\mathbf{x}) = 1/x_1 + (1378000000x_2^3x_3(((x_1^3(4x_1^2(680\pi(2x_4 + 2x_5)(x_6^2 \\ - x_7^2) + 0.895) \\ + (21760x_1^3x_2x_3)/3))/(55120000x_2^3x_3) - 1)^2 \\ + x_1^6/(47472100000000x_2^6x_3^2))^{1/2})/x_1^3, \end{aligned}$$

and the constraints are:

$$\begin{aligned} g_1(\mathbf{x}) = (9x_1^3)/(17225000x_2^3x_3\pi(((x_1^3(4x_1^2(680\pi(2x_4 \\ + 2x_5)(x_6^2 - x_7^2) + 0.895) \\ + (21760x_1^3x_2x_3)/3)) \\ /(55120000x_2^3x_3) - 1)^2 \\ + x_1^6 \\ /(47472100000000x_2^6x_3^2))^{1/2}) - 1 \\ \le 0, \end{aligned} \tag{7}$$
$$g_2(\mathbf{x}) = \frac{x_3}{x_2} - 1 \le 0, \quad g_3(\mathbf{x}) = \frac{x_7}{x_6} - 1 \le 0,$$
$$g_4(\mathbf{x}) = x_6 - x_7 - 0.002 = 0,$$
$$g_5(\mathbf{x}) = x_5 - x_4 - 1 \le 0,$$

in which the bounds of variables are $0.4 \le x_1 \le 0.6$, $0.01 \le x_2 \le 0.02$, $0.002 \le x_3 \le 0.006$, $0.1 \le x_4 \le 0.18$, $0.1 \le x_5 \le 0.18$, $0.004 \le x_6 \le 0.012$, and $0.002 \le x_7 \le 0.008$. Now the task is to minimize the cost function (6) subjected to constraints (7).

IV. Optimization Algorithm

The applied optimization algorithm for the constrained problem was introduced recently for solving engineering optimization problems [27]. The method works by shooting random solutions in the search domain, next, obtaining the best answer, then reducing the search zone around the last answer. Keeping the same procedure and reducing the zones result in an intelligent zooming mechanism that provides the optimal solution. The method works based on the definition of zones. The cost function is a general nonlinear function, not necessarily convex such as $F(\mathbf{x})$ for optimization where $\mathbf{x} =$

This is the preprint version of the article:
S. R. Nekoo, A. Suarez, J. Á. Acosta, G. Heredia and A. Ollero, "Constrained Design Optimization of a Long-Reach Dual-Arm Aerial Manipulator for Maintenance Tasks," 2023 International Conference on Unmanned Aircraft Systems (ICUAS), Warsaw, Poland, 2023, pp. 281-288, doi: 10.1109/ICUAS57906.2023.10156252.

$[x_1, x_2, \dots, x_n]^T$ in which n is the number of variables. The first zone is the entire search space between $\mathbf{x}_{\min} \leq \mathbf{x} \leq \mathbf{x}_{\max}$:

$$x_p(i) = \text{rand}[0,1]\left(x_{\max,p} - x_{\min,p}\right) + x_{\min,p}, \tag{8}$$

where $\text{rand}[0,1]$ generates a random number between 0 and 1, $p = 1, \dots, n$, and index i is the counter of generations of solutions. The random solutions in the first zone are tried and checked with the cost function. In each iteration, if the current answer is better than the previous one, the algorithm records the solution and goes to another generation. The method repeats this task for N_1 times; in each zone the iteration numbers are $N_1, \dots, N_r, \dots, N_Z$ where Z is the total number of zones. The last generated answer so far is the best one, hence, the search zone is reduced around the last solution in zone r:

$$x_p(i) = \text{rand}[0,1]\left(x_{\max,p,N_r} - x_{\min,p,N_r}\right) + x_{\min,p,N_r}, \tag{9}$$

where

$$x_{\max,p,N_r} = x_p(i-1) + \frac{\left(x_{\max,p} - x_{\min,p}\right)}{2P_r}, \tag{10}$$

$$x_{\min,p,N_r} = x_p(i-1) - \frac{\left(x_{\max,p} - x_{\min,p}\right)}{2P_r}, \tag{11}$$

in which P_r is a reduction percentage of r-th zone with the following condition holds:

$$\begin{aligned} &\text{if} \quad x_{\max,p,N_r} > x_{\max,p}, \quad x_{\max,p,N_r} = x_{\max,p}, \\ &\text{if} \quad x_{\min,p,N_r} < x_{\min,p}, \quad x_{\min,p,N_r} = x_{\min,p}. \end{aligned}$$

The pseudocode of the algorithm is presented Ref. [27]. There are two counters, i for generations of solutions, and j for iterations. More details of the algorithm, the probabilistic formula of the evolution, and the flowchart could be found in Ref. [27].

V. Particle Swarm Optimization

Particle swarm optimization is a search method for solving optimization problems without any restriction to the form of the cost function, it is not limited to convex/concave form, complexity, or the number of constraints. It was introduced by Kennedy and Eberhart in 1995 [31], combined and reinforced by many types, and applied to a variety of optimization problems [32, 33]. Here the basic idea of PSO is briefly revisited for validation of the results. The PSO first sweeps randomly all the search space, using Eq. (8), and introduces the particle best cost (choosing the minimum cost function $F(\mathbf{x})$ among the trials) and the particle best position so far. In another loop, the next phase is to update the particle position by:

$$x_p(i+1) = x_p(i) + v_p(i+1),$$

where $p = 1, \dots, n$; $x_p(i)$ is the position of the particle and $v_p(i)$ is the velocity of the particle p at i-th step. The velocity rule is [34]:

$$v_p(i+1) = wv_p(i) + c_1 r_1 \left(\hat{x}_p(i) - x_p(i)\right) + c_2 r_2 \left(g_p(i) - x_p(i)\right),$$

where $\hat{x}_p(i)$ is the individual best candidate and $g_p(i)$ is the swarm's global best candidate. The constant parameters are $0 < w < 1.2$, $0 < c_1 < 2$ and $0 < c_2 < 2$ could be chosen. The parameters r_1 and r_2 are random numbers between $(0,1)$, generated at each step. $wv_p(i)$ is an inertia component that urges the particle to move in the original direction, $c_1 r_1 \left(\hat{x}_p(i) - x_p(i)\right)$ is a cognitive component that urges the particle to revisit regions with high individual fitness, and $c_2 r_2 \left(g_p(i) - x_p(i)\right)$ is a social component that causes the particle to wander around the global best position so far, and more details could be found in Ref. [35]. Velocity clamping is also applied to limit the particle from going too far from the region [34]: $v_{\max,\min} = \pm \frac{k(x_{\max} - x_{\min})}{2}$, in which $0.1 < k < 1$ is the velocity clamping constant.

VI. Simulation and Results

The proposed search algorithm in Section IV is implemented on cost function (6) subjected to constraints (7) within the allowable domain of variables. The parameters of the method are considered by setting $Z = 8$ zones with

$$N = [500, 1000, 1500, 2000, 2500, 3000, 3500, 4000],$$

and reduction zone percentage

$$P = [0.5, 0.25, 0.1, 0.01, 0.005, 0.001, 0.0001],$$

The nominal value of the current design for the variables is

$$\mathbf{x}_{\text{nom}} = [0.5, 0.015, 0.002, 0.11, 0.14, 0.006, 0.004]^T,$$

which defines $M_{\text{nom}} = 1\,\text{kg}$ total weight of the nominal system and workspace $W_{\text{nom}} = 0.897841000457183(\text{m}^3)$. The new cost function aims to increase the workspace with a trade-off between weight and imposed vibration. The allowable bound of vibration was defined $\theta_{\max} = 0.25^{\circ}$ and the maximum actual vibration with the obtained new parameters is found $[\theta_{\text{actual}}]_{\max} = 0.249999970181408^{\circ}$. The optimized workspace is gained $W = 1.876174204226$ $(\text{m}^3)$and the weight of the new system is $M = 1.183398913$ (kg). The improvement in the workspace is 108.9% and the increase in weight is 18.33%. It is not possible to increase the workspace without additional weight though the rate of workspace improvement concerning the increase of weight is properly defined. The details of the cost function values are reported in Table 3. The flow of the solutions is illustrated in Fig. 8. The configuration of the robot and the optimal workspace are presented in Fig. 9. reported in Table 3. From the results from Table 3, to compare and validate the approach, the PSO is also implemented on the optimization problem. The parameters of the PSO were selected as $w = 1.2$, $c_1 = 1.8$, $c_2 = 1.5$, $k = 1$, the inner loop $N_i = 100$ and the outer loop $N_j = 1000$. The global best cost was gained 232.227802870688 with 0.02 standard deviation for 30 trials, reported in Table 3. From the results from Table 3, it can be seen that the PSO gained less standard deviation and that shows more steadiness in the solution. The nominal parameters of the arm resulted in 1 (kg) total weight. After

This is the preprint version of the article:
S. R. Nekoo, A. Suarez, J. Á. Acosta, G. Heredia and A. Ollero, "Constrained Design Optimization of a Long-Reach Dual-Arm Aerial Manipulator for Maintenance Tasks," 2023 International Conference on Unmanned Aircraft Systems (ICUAS), Warsaw, Poland, 2023, pp. 281-288, doi: 10.1109/ICUAS57906.2023.10156252.

optimization, the nominal weight increased by 0.18 (kg) and an increase in the workspace by almost 100%. The long-reach design was also enhanced by 4 (cm) by PSO and 10 (cm) by the proposed approach which increases the safety measurements in contact with high-voltage power lines. These new parameters will be used in redesigning the final prototype which is the objective of this work.

Table 3. Details of cost function values and optimized parameters in 30 trials.

method	**x**	$f(\mathbf{x})$				SD
		best	median	mean	worst	
PSO	[0.539996856163741, 0.02, 0.002, 0.177870928297851, 0.160256378885885, 0.006, 004]	232.227802870688	232.258264153966	232.260983950301	232.309695117708	0.02
Ref. [27]	[0.599938313517637, 0.018, 0.004, 0.176103127661595, 0.171171102118409, 0.01, 0.008]	232.166632223409	232.329641988104	232.373398260586	232.817693303755	0.08

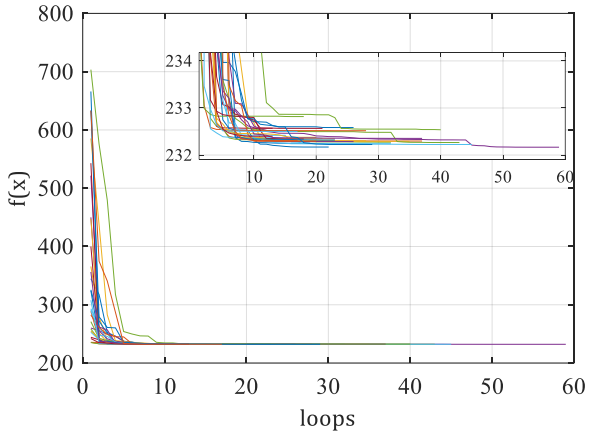

Fig. 8. Convergence of the search algorithm' solution for the optimization problem.

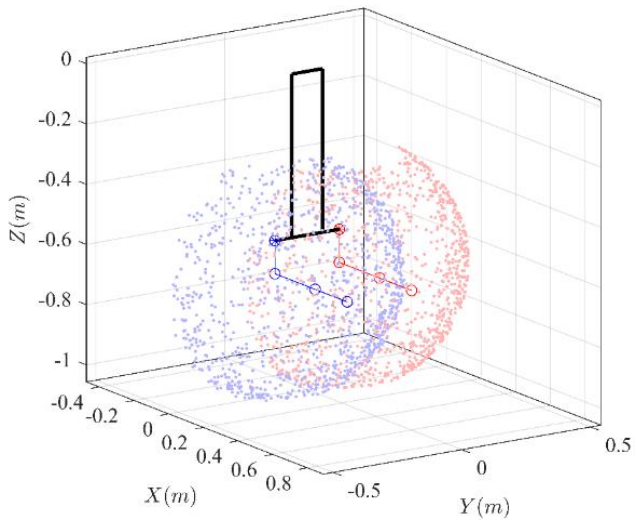

Fig. 9. The configuration of the robot and optimal workspace.

VII. Conclusions

Inspection of high-voltage power lines preferably requires remote tools to reduce the risk factors of working conditions for human operators to the lowest possible rate. A popular tool for inspection is multirotor drones that could perform stable and stationary flights. They are also cost-efficient and lightweight. The power lines impose a strong magnetic field on the drone and might risk communication with a ground station. So, the idea of the long-reach manipulator was introduced to increase the distance between the drone and the inspection/manipulation area. The aerial manipulator must be lightweight and also robust in terms of imposed vibration. The design of such a system possesses so many variables, objectives, and constraints. An extensive study was done the generate the cost function and constraints of the design for performing the optimization. A search algorithm was used to find the best answer. The simulation proposed a 108.9% increase in the workspace and an 18.33% increase in weight. The solution was also validated by particle swarm optimization which gained almost the same result, though the minimum value of the cost function was scored by the introduced method in Ref. [27]. The nominal parameters of the arm resulted in 1 (kg) total weight and by optimization, it increased to 0.18 (kg) with almost 100% of the workspace. The long-reach design was also enhanced by 4 (cm) by PSO and 10 (cm) by the search algorithm. The objective of this work was to find the optimum parameter definition based on a logical cost function to increase the workspace and long-reach condition at the lowest possible cost (increase in weight). The data and results of this work will be used in redesigning the ultimate prototype of this research.

Acknowledgments

This work was supported by the AERIAL-CORE Project of the European Commission under Grant H2020-2019-871479; and HAERA (Spanish Ministry of Science and Innovation PID2020-119027RB-I00).

The research work of Alejandro Suarez is supported by the Consejería de Transformación Económica, Industria, Conocimiento y Universidades de la Junta de Andalucía (Spain) through a post-doctoral research grant.

This is the preprint version of the article:
S. R. Nekoo, A. Suarez, J. Á. Acosta, G. Heredia and A. Ollero, "Constrained Design Optimization of a Long-Reach Dual-Arm Aerial Manipulator for Maintenance Tasks," 2023 International Conference on Unmanned Aircraft Systems (ICUAS), Warsaw, Poland, 2023, pp. 281-288, doi: 10.1109/ICUAS57906.2023.10156252.

REFERENCES

[1] A. Ollero, M. Tognon, A. Suarez, D. Lee and A. Franchi, "Past, Present, and Future of Aerial Robotic Manipulators," in *IEEE Transactions on Robotics*, vol. 38, no. 1, pp. 626-645, Feb. 2022.

[2] F. Ruggiero, V. Lippiello, and A. Ollero, "Aerial manipulation: A literature review," *IEEE Robotics and Automation Letters*, vol. 3, pp. 1957-1964, 2018.

[3] A. Rodriguez-Castaño, S. R. Nekoo, H. Romero, R. Salmoral, J. Á. Acosta, and A. Ollero, "Installation of clip-type bird flight diverters on high-voltage power lines with aerial manipulation robot: Prototype and testbed experimentation," *Applied Sciences*, vol. 11, p. 7427, 2021.

[4] M. Tognon, H. A. T. Chávez, E. Gasparin, Q. Sablé, D. Bicego, A. Mallet, *et al.*, "A truly-redundant aerial manipulator system with application to push-and-slide inspection in industrial plants," *IEEE Robotics and Automation Letters*, vol. 4, pp. 1846-1851, 2019.

[5] M. Á. Trujillo, J. R. Martínez-de Dios, C. Martín, A. Viguria, and A. Ollero, "Novel aerial manipulator for accurate and robust industrial NDT contact inspection: A new tool for the oil and gas inspection industry," *Sensors*, vol. 19, p. 1305, 2019.

[6] H. W. Wopereis, J. J. Hoekstra, T. H. Post, G. A. Folkertsma, S. Stramigioli, and M. Fumagalli, "Application of substantial and sustained force to vertical surfaces using a quadrotor," in *2017 IEEE international conference on robotics and automation (ICRA)*, 2017, pp. 2704-2709.

[7] A. Suarez, F. Real, V. M. Vega, G. Heredia, A. Rodriguez-Castaño, and A. Ollero, "Compliant bimanual aerial manipulation: Standard and long reach configurations," *IEEE Access*, vol. 8, pp. 88844-88865, 2020.

[8] M. Orsag, C. Korpela, S. Bogdan, and P. Oh, "Valve turning using a dual-arm aerial manipulator," in *2014 international conference on unmanned aircraft systems (ICUAS)*, 2014, pp. 836-841.

[9] S. Shimahara, S. Leewiwatwong, R. Ladig, and K. Shimonomura, "Aerial torsional manipulation employing multi-rotor flying robot," in *2016 IEEE/RSJ International Conference on Intelligent Robots and Systems (IROS)*, 2016, pp. 1595-1600.

[10] T. Ikeda, S. Yasui, M. Fujihara, K. Ohara, S. Ashizawa, A. Ichikawa, *et al.*, "Wall contact by octo-rotor UAV with one DoF manipulator for bridge inspection," in *2017 IEEE/RSJ International Conference on Intelligent Robots and Systems (IROS)*, 2017, pp. 5122-5127.

[11] G. Gioioso, A. Franchi, G. Salvietti, S. Scheggi, and D. Prattichizzo, "The flying hand: A formation of UAVs for cooperative aerial tele-manipulation," in *2014 IEEE International conference on robotics and automation (ICRA)*, 2014, pp. 4335-4341.

[12] H. Seo, S. Kim, and H. J. Kim, "Aerial grasping of cylindrical object using visual servoing based on stochastic model predictive control," in *2017 IEEE international conference on robotics and automation (ICRA)*, 2017, pp. 6362-6368.

[13] A. Suarez, P. R. Soria, G. Heredia, B. C. Arrue, and A. Ollero, "Anthropomorphic, compliant and lightweight dual arm system for aerial manipulation," in *2017 IEEE/RSJ International Conference on Intelligent Robots and Systems (IROS)*, 2017, pp. 992-997.

[14] A. Suarez, A. E. Jimenez-Cano, V. M. Vega, G. Heredia, A. Rodriguez-Castaño, and A. Ollero, "Design of a lightweight dual arm system for aerial manipulation," *Mechatronics*, vol. 50, pp. 30-44, 2018.

[15] S. R. Nekoo, J. R. Acosta, G. Heredia, and A. Ollero, "Soft-landing of multi-rotor drones using a robust nonlinear control and wind modeling*," in *2021 International Conference on Unmanned Aircraft Systems (ICUAS)*, Athens, Greece, 2021.

[16] S. R. Nekoo, P. J. S. Cuevas, J. Á. Acosta, G. Heredia, and A. Ollero, "Experimental investigation of soft-landing of quadrotors via induced wind modeling approach," in *2021 Aerial Robotic Systems Physically Interacting with the Environment (AIRPHARO)*, Biograd na Moru, Croatia, 2021, pp. 1-6.

[17] C. Wisniewski and K. Van Treuren, "Novel UAS propeller design part 1: Using an unloaded tip to reduce power requirements and lower generated sound levels for propellers designed for minimum induced drag," in *Turbo Expo: Power for Land, Sea, and Air*, 2022, p. V001T01A012.

[18] P. Tseng and S. Yun, "A coordinate gradient descent method for nonsmooth separable minimization," *Mathematical Programming*, vol. 117, pp. 387-423, 2009.

[19] S. Ceria and J. Soares, "Convex programming for disjunctive convex optimization," *Mathematical Programming*, vol. 86, pp. 595-614, 1999.

[20] Y.-H. Liu, "Qualitative test and force optimization of 3-D frictional form-closure grasps using linear programming," *IEEE Transactions on Robotics and Automation*, vol. 15, pp. 163-173, 1999.

[21] A. Öcal and H. Koyuncu, "Optimum design of flapping wing flying robot by modified social group optimization," in *2022 13th International Conference on Computing Communication and Networking Technologies (ICCCNT)*, Kharagpur, India, 2022, pp. 1-5.

[22] L. Bianchi, M. Dorigo, L. M. Gambardella, and W. J. Gutjahr, "A survey on metaheuristics for stochastic combinatorial optimization," *Natural Computing*, vol. 8, pp. 239-287, 2009.

[23] M. Ghosh, S. Begum, R. Sarkar, D. Chakraborty, and U. Maulik, "Recursive memetic algorithm for gene selection in microarray data," *Expert Systems with Applications*, vol. 116, pp. 172-185, 2019.

[24] A. L. Alfeo, M. G. C. A. Cimino, and G. Vaglini, "Enhancing biologically inspired swarm behavior: Metaheuristics to foster the optimization of UAVs coordination in target search," *Computers & Operations Research*, vol. 110, pp. 34-47, 2019.

[25] G. B. Mahanta, A. Rout, B. B. V. L. Deepak, and B. B. Biswal, "Application of meta-heuristic optimization techniques for design optimization of a robotic gripper," *International Journal of Applied Metaheuristic Computing* vol. 10, pp. 107-133, 2019.

[26] J.-G. J. Durand, F. Burgaud, K. D. Cooksey, and D. N. Mavris, "A design optimization technique for multi-robot systems," in *55th AIAA Aerospace Sciences Meeting*, 2017, p. 0690.

[27] S. R. Nekoo, J. A. Acosta, and A. Ollero, "A search algorithm for constrained engineering optimization and tuning the gains of controllers," *Expert Systems with Applications*, vol. 206, 2022.

[28] A. Suárez, P. Sanchez-Cuevas, M. Fernandez, M. Perez, G. Heredia, and A. Ollero, "Lightweight and compliant long reach aerial manipulator for inspection operations," in *2018 IEEE/RSJ International Conference on Intelligent Robots and Systems (IROS)*, 2018, pp. 6746-6752.

[29] I. Palunko, R. Fierro, and P. Cruz, "Trajectory generation for swing-free maneuvers of a quadrotor with suspended payload: A dynamic programming approach," in *2012 IEEE International Conference on Robotics and Automation*, 2012, pp. 2691-2697.

[30] Y. S. Sarkisov, M. J. Kim, D. Bicego, D. Tsetserukou, C. Ott, A. Franchi, *et al.*, "Development of sam: cable-suspended aerial manipulator," in *2019 International Conference on Robotics and Automation (ICRA)*, 2019, pp. 5323-5329.

[31] J. Kennedy and R. Eberhart, "Particle swarm optimization," in *Proceedings of ICNN'95-International Conference on Neural Networks*, 1995, pp. 1942-1948.

[32] A. Banks, J. Vincent, and C. Anyakoha, "A review of particle swarm optimization. Part I: background and development," *Natural Computing*, vol. 6, pp. 467-484, 2007.

[33] A. Banks, J. Vincent, and C. Anyakoha, "A review of particle swarm optimization. Part II: hybridisation, combinatorial, multicriteria and constrained optimization, and indicative applications," *Natural Computing*, vol. 7, pp. 109-124, 2008.

[34] F. Van Den Bergh and A. P. Engelbrecht, "A study of particle swarm optimization particle trajectories," *Information sciences*, vol. 176, pp. 937-971, 2006.

[35] A. Tharwat, T. Gaber, A. E. Hassanien, and B. E. Elnaghi, "Particle swarm optimization: a tutorial," in *Handbook of research on machine learning innovations and trends*, ed: IGI global, 2017, pp. 614-635.